Investigation of Microstructure and Photoluminescence of Ce^{3+}/Eu^{3+} Codoped $KZnPO_4$ Phosphors

Guan-Ping Qi,[1] Huang Sheng Lai,[2] Shoou-Jinn Chang,[3] and Ru-Yuan Yang[4*]

[1]Institute of Microelectronics, National Cheng Kung University,
No. 1 University Road, East Area, Tainan City 701, Tainan County
[2]Department of Materials, National Pingtung University of Science and Technology,
No. 1 Shuefu Road, Nuipu Area, Pingtung City 912, Pingtung County
[3]Institute of Microelectronics, National Cheng Kung University,
No. 1 University Road, East Area, Tainan City 701, Tainan County
[4]Department of Materials National Pingtung University of Science and Technology,
No. 1 Shuefu Road, Nuipu Area, Pingtung City 912, Pingtung County

The solid-state reaction method was used to prepare Ce^{3+}/Eu^{3+} codoped $KZnPO_4$ phosphors for white light-emitting diodes (W-LEDs). The phase formation of Ce^{3+}/Eu^{3+} codoped $KZnPO_4$ was verified by X-ray powder diffraction (XRD) analysis. Under excitation at around 395 nm, red emission corresponding to the $^5D_0 \rightarrow {}^7F_2$ transition was observed from Ce^{3+}/Eu^{3+} codoped $KZnPO_4$ phosphors. The codoped Ce^{3+} in $KZnPO_4$:Eu^{3+},Ce^{3+} affects the microstructural symmetry because of different ionic sizes, leading to the different emission properties of $KZnPO_4$:Eu^{3+}. The codoping method may be efficient for adjusting the luminous characteristics of phosphors.

1. Introduction

The white light-emitting diode (WLED) is a well-known mercury-free lighting source. Compared with traditional light sources, WLED has the advantages of small size, energy savings, long life, low heat generation, and good response speed. Therefore, WLED has the potential to be developed into the mainstream of lighting equipment.[1–4] The phosphors used in LEDs are common to light conversion materials, which absorb light of various wavelength bands and emit light at specific wavelengths governed by the excited energy levels of the ions. Accordingly, they play an essential role in WLEDs excited by a single chip, multichip, blue chip, or an ultraviolet chip.[5] However, some features such as high luminescent efficiency, stability, and low cost are requested for phosphors applied in WLEDs.

The phosphate compounds with the general composition $ABPO_4$ (A = alkali metals and B = alkaline earth metals) are ideal host materials. The excellent thermal stability of $ABPO_4$ compounds owing to charge stabilization is a result of the rigid tetrahedral three-dimensional matrix of phosphate. In the past, $ABPO_4$ compounds doped with different types of rare-earth

ions (e.g., Eu^{3+}, Ce^{3+}, Tb^{3+}, and Sm^{3+}.) were frequently reported in the literature,[6–8] where Eu^{3+} and Ce^{3+} ions are two impressionable earth ions used to generate red and blue emissions under UV excitation. According to Laporte parity selection rules, the allowed 4f–5d transitions of the Ce^{3+} ion make it act as a highly efficient emission center. Ce^{3+} is a very good candidate for a sensitizer for the UV excitation of Eu^{3+} in such phosphate lattices. Thus, many Ce^{3+} and Eu^{3+} codoped phosphors have been reported and prepared, such as $Tb_3Al_5O_{12}$:Ce^{3+},Eu^{3+};[9] $Ca_2MgSi_2O_7$:Ce^{3+}/Eu^{3+};[10] Li_2BaZrO_4:Ce^{3+}/Eu^{3+};[11] and $K_3Gd_5(PO_4)_6$:Eu^{3+}/Ce^{3+}.[12] However, there is no report on the microstructure or luminescent characteristics of $KZnPO_4$ codoped with Ce^{3+} and Eu^{3+}. There is a probability of energy transfer between Ce^{3+} and Eu^{3+} in the $KZnPO_4$ host. In the present work, a series of $KZn_{1-x-y}PO_4$:xEu^{3+}:yCe^{3+} phosphors were synthesized by the solid-state reaction technique. X-ray diffraction (XRD), scanning electron microscopy (SEM), and photoluminescence (PL) measurements were used to investigate the microstructure and luminescent characteristics of $KZnPO_4$:Ce^{3+},Eu^{3+} phosphors. The codoping effect on the microstructure was also considered in this study.

2. Materials and Methods

From previous studies,[13–15] the optimal Eu concentration in Eu-doped $KZnPO_4$ has been found to be 0.04 in the chemical formula $KZn_{0.96}PO_4$:$0.04Eu^{3+}$. Therefore, in this work, a series of $KZnPO_4$-based phosphors codoped with Ce^{3+} and Eu^{3+} were synthesized by conventional solid-state sintering according to $KZn_{1-x-y}PO_4$:xEu^{3+}:yCe^{3+} with the Eu^{3+} concentration fixed at $x = 0.04$. The raw materials used, including potassium carbonate (K_2CO_3, Alfa Aesar), zinc oxide (ZnO, Alfa Aesar), and ammonium dihydrogen phosphate ($NH_4H_2PO_4$, Alfa Aesar), were of analytical reagent grade, while the purities of Ce_2O_3 and Eu_2O_3 were higher than 99.99%. The powders of potassium carbonate, zinc oxide, ammonium dihydrogen phosphate, and activator (Eu, Ce) were mixed in an appropriate ratio, and the doping concentration of Ce^{3+} was taken to be equal to $y = 0.003$, 0.007, 0.01, or 0.03. The powder mixture was inserted into a plastic bottle to which absolute ethanol and zirconia balls of different diameters were added. Then, the plastic bottle was installed on a ball mill for ball milling at 400 rpm for 1 h. After ball milling, the solution was poured out from the plastic bottle and put into the oven for drying at 70 °C, as shown in Fig 1. The powder was placed in an alumina crucible for sintering in a furnace at a constant heating rate of 10 °C/min from 900 to 1300 °C for 3 h. X-ray diffraction (XRD) [XRD-7000S diffractometer with Cu Kα radiation ($\lambda = 0.15374$ nm) operating at 40 kV and 20 mA] was used to characterize the microstructure of the phosphors. The data were collected with a step of 0.02° (2 theta) and a count time of 1 s per step. The particle morphology was observed using a HITACHI SU-5000 scanning electron microscopy (SEM) system. The photoluminescence, excitation, and emission spectra were recorded with an FP-6600 fluorescence spectrophotometer.

3. Results

Figure 2(a) shows the XRD diffraction patterns of $KZn_{0.957}PO_4$:$0.04Eu^{3+}$:$0.003Ce^{3+}$ phosphors synthesized at different temperatures. Judging from the Joint Committee on Powder
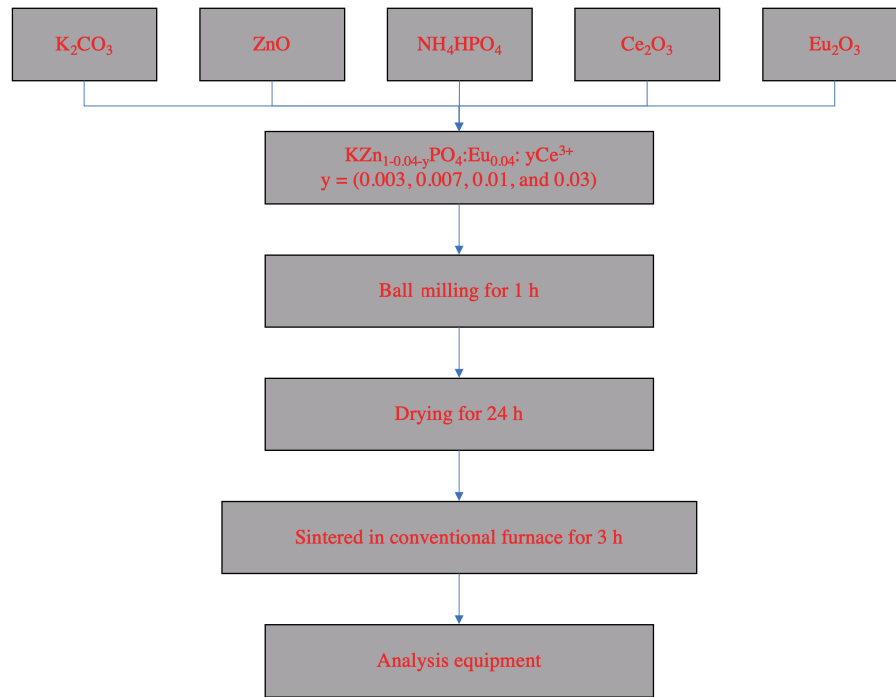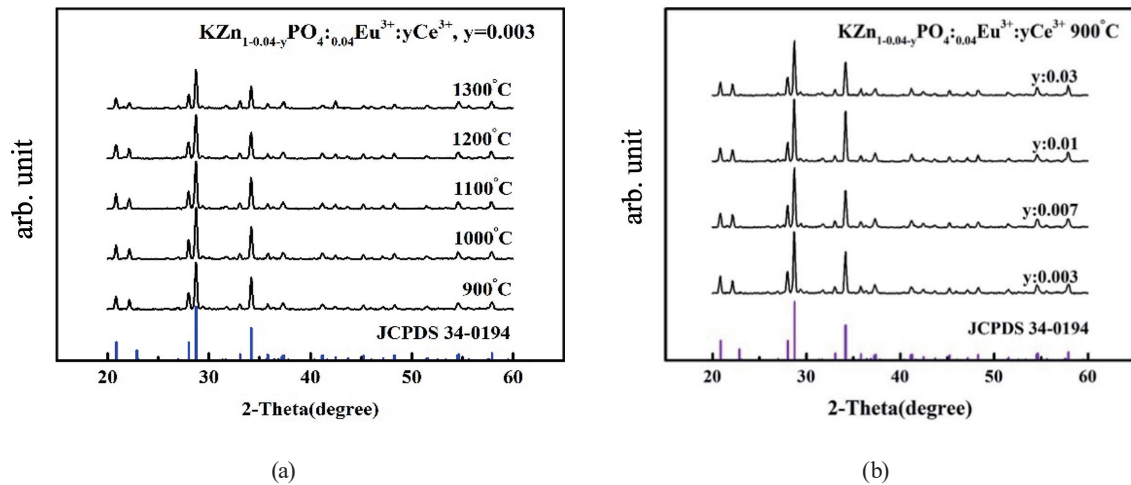
Fig. 1.   (Color online) Main steps of the experiment.

(a)

(b)

Fig. 2.   (Color online) (a) XRD diffraction patterns of $KZn_{0.957}PO_4:0.04Eu^{3+}:yCe^{3+}$, $y = 0.003$ phosphors fabricated at different sintering temperatures. (b) XRD diffraction patterns of $KZn_{0.96-y}PO_4:0.04Eu^{3+}:yCe^{3+}$ phosphors ($y = 0.003$, 0.007, 0.01, and 0.03) sintered at 900 °C.

Diffraction Standards (JCPDS #34-0194), the cell parameter and volume changed little with the substitution of Eu and Ce. We suggest that the activator and coactivator (Eu^{3+} and Ce^{3+}) have been incorporated into the lattice. Considering the effect of the ionic sizes of cations, we propose that Ce^{3+} (1.02 Å) and Eu^{3+} (0.95 Å) ions are expected to preferably occupy Zn^{2+} (0.74 Å) sites, not K^+ (1.38 Å) sites. Therefore, there was no detectable shift in the XRD spectrum. Additionally,

the $KZn_{1-0.04-y}PO_4$:0.04Eu^{3+}:yCe^{3+} (y = 0.003) phosphors prepared at 900, 1000, 1100, 1200, and 1300 °C all have a hexagonal structure with cell parameters $a = b = 18.16$ Å, $c = 8.506$ Å, $\alpha = \beta = 90°$, $\gamma = 120°$, $Z = 24$, and $V = 2431.2$ (Å)^3.[15] As the sintering temperature increases from 900 to 1300 °C, the XRD analysis shows that no secondary phase was generated. Figure 2(b) shows the XRD diffraction patterns of $KZn_{0.96-y}PO_4$:0.04Eu^{3+}:yCe^{3+} phosphors with different Ce^{3+} concentrations sintered at 900 °C. As seen, no secondary phase was formed with increasing Ce^{3+} ion concentration. Because the ion radius of Ce^{3+} (1.02 Å) is larger than that of Zn^{2+} (0.74 Å), with increasing Ce^{3+} ion concentration, the diffraction peak shifted slightly toward the lower angle direction. A higher crystallinity in the XRD spectra can be inferred from the full width at half-maximum (FWHM) and intensity of the diffraction peaks. As the sintering temperature increased to 1300 °C, the FWHM and intensity of the diffraction peaks of the prepared $KZn_{1-0.04-y}PO_4$:0.04Eu^{3+}:0.003Ce^{3+} became broad and low, respectively, indicating poor crystallinity. Furthermore, the FWHM and intensity of the diffraction peaks of $KZn_{0.96-y}PO_4$:0.04Eu^{3+}:yCe^{3+} phosphors with different Ce^{3+} concentrations sintered at 900 °C were similar, indicating all samples having similar crystallinities.

The luminescence intensity of phosphor is usually affected by the particle size distribution.[16] Figures 3(a) to 3(e) show the SEM images of $KZn_{0.957}PO_4$:0.04Eu^{3+}:0.003Ce^{3+} synthesized at

(a)

(b)

(c)

(d)
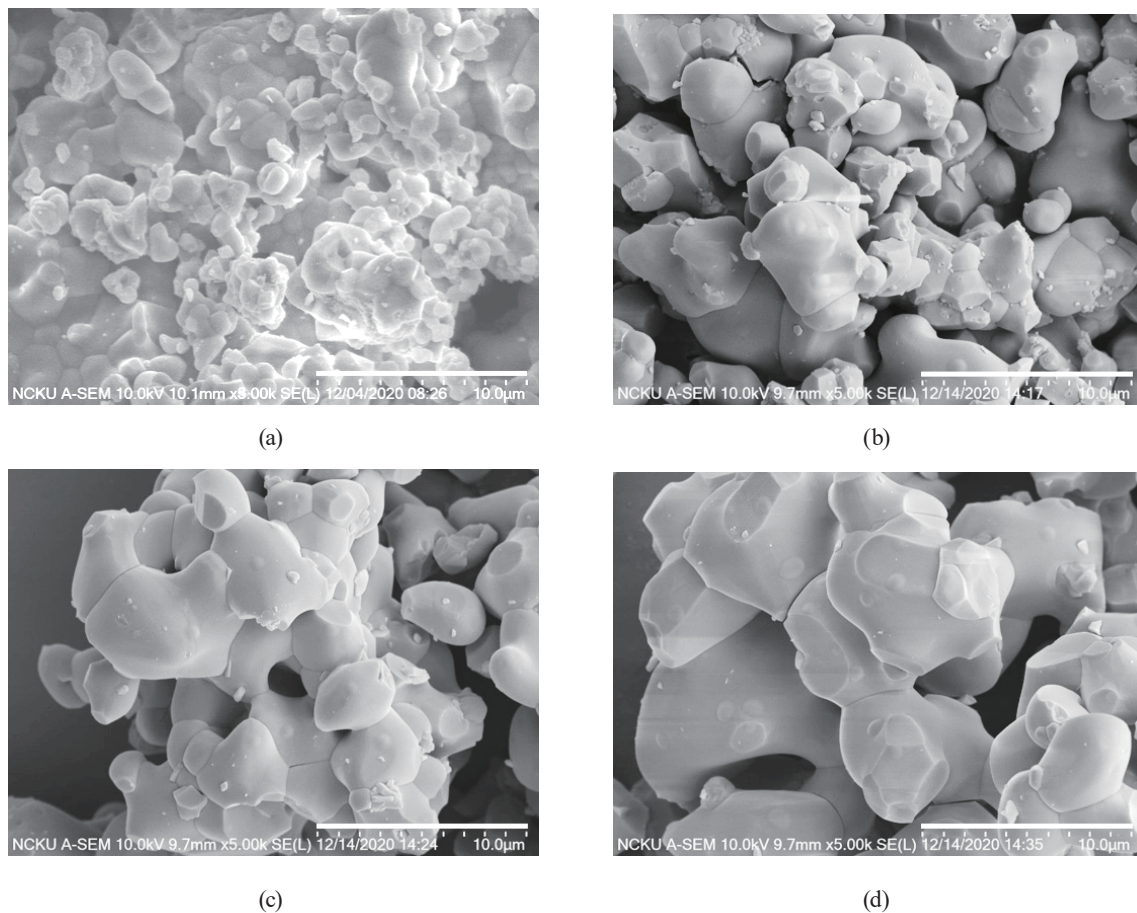
Fig. 3.   SEM images of $KZn_{0.957}PO_4$:0.04Eu^{3+}:0.003Ce^{3+} sintered at (a) 900, (b) 1000, (c) 1100, (d) 1200, and (e) 1300 °C, and SEM images of $KZn_{0.96-y}PO_4$:0.04Eu^{3+}:yCe^{3+} phosphors with different Ce^{3+} concentrations of (f) y = 0.003 and (g) y = 0.03 sintered at 900 °C.

(e)

(f)

(g)

Fig. 3. (Continued) SEM images of $KZn_{0.957}PO_4$:$0.04Eu^{3+}$:$0.003Ce^{3+}$ sintered at (a) 900, (b) 1000, (c) 1100, (d) 1200, and (e) 1300 °C, and SEM images of $KZn_{0.96-y}PO_4$:$0.04Eu^{3+}$:yCe^{3+} phosphors with different Ce^{3+} concentrations of (f) $y = 0.003$ and (g) $y = 0.03$ sintered at 900 °C.

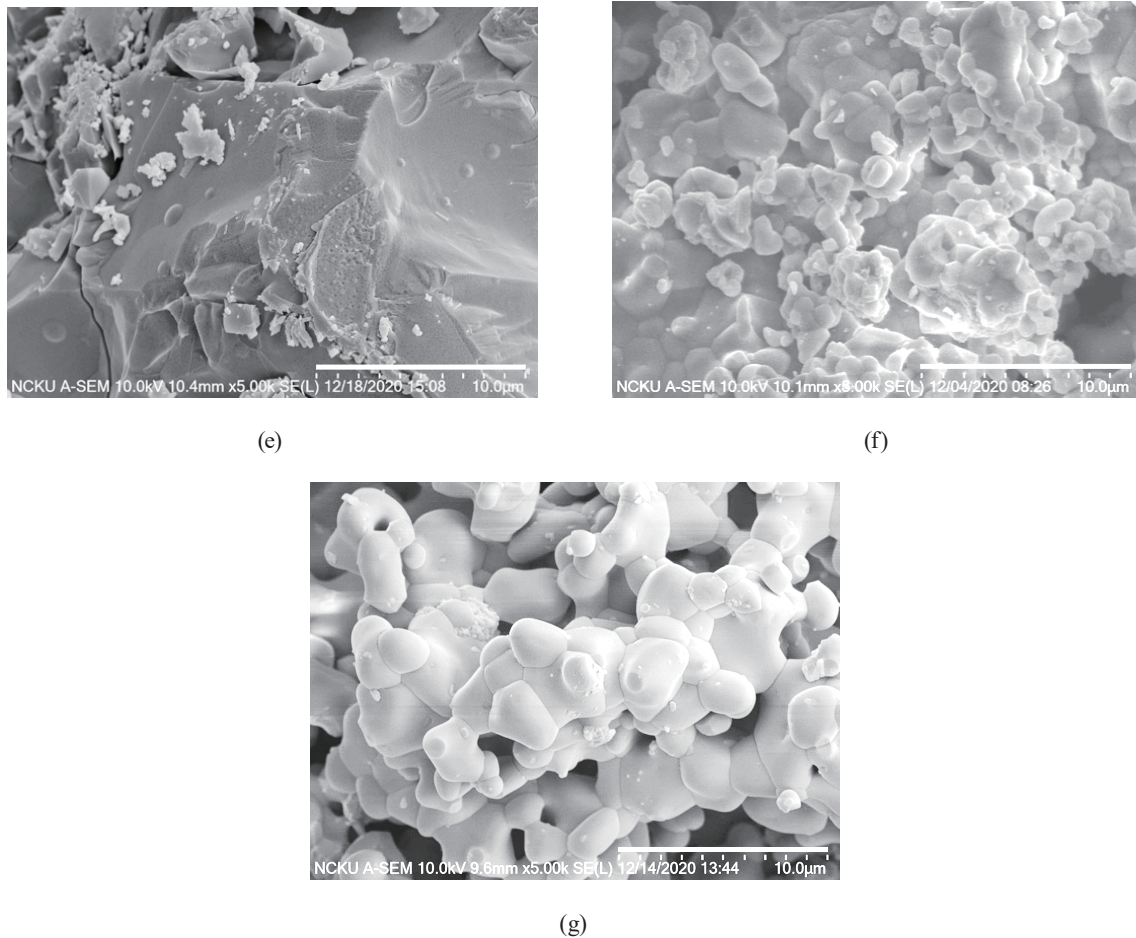different sintering temperatures. As the sintering temperature increases, the particle size increases from 4 to 13.7 μm or more and the particle shape changes from spherical to plate-like. The grains are highly coalescent, which indicates the strong interdiffusion of the grain components. Commonly, such grain morphology is related to high crystallinity and chemical uniformity. Earlier, a similar morphology type was observed in different oxide compounds subjected to high-temperature treatment.[17–19] As the sintering temperature becomes higher than 1300 °C, the melting phenomenon seems to occur around the crystal grains, and the crystallinity becomes poor, as verified by XRD measurements. Figures 3(f) and 3(g) show SEM images of $KZn_{0.96-y}PO_4$:$0.04Eu^{3+}$:yCe^{3+} phosphors with different Ce^{3+} concentrations sintered at 900 °C. As the codoping concentration increases, the grain size tends to increase from 4 to above 15 μm because the higher Ce^{3+} concentration increases the lattice parameter of the $KZnPO_4$ phosphor.

4. Discussion

The red light emitted upon the $^5D_0 \rightarrow {}^7F_1$ magnetic dipole transition (591 nm) and $^5D_0 \rightarrow {}^7F_2$ electric dipole transition (616 nm)[20] originated from Eu^{3+} rare-earth ions. Therefore, the codoping of Eu^{3+} ions can act as a red emission compensation for white light. Figure 4(a) shows the PL excitation spectra of the $KZn_{0.957}PO_4:0.04Eu^{3+}:0.003Ce^{3+}$ phosphor sintered at different temperatures (λ_{em} = 596 nm). The most intense excitation band is between 300 and 450 nm, and six components are identified in the excitation spectra, which can be assigned to the intraconfigurational 4f–4f transitions of Eu^{3+} ions, including $^7F_0 \rightarrow {}^5D_4$ at 362 nm, $^7F_0 \rightarrow {}^5L_7$ at 381 nm, $^7F_0 \rightarrow {}^5L_6$ at 394 nm, and $^7F_0 \rightarrow {}^5D_3$ at 415 nm.[21–23] For wavelengths below 350 nm, a broadband is perceived, which is likely to be due to host matrix absorption.[24] For $KZnPO_4:Eu^{3+}$, a wide band in the UV region centered at about 200–271 nm corresponds to the charge transfer state (CTS) band of europium–oxygen interactions.[15] However, in this study, for $KZnPO_4$ codoped with Eu^{3+}/Ce^{3+}, the prominent excitation peak at 394 nm is suitable for ultraviolet light chip excitation, so this wavelength is selected for the measurement of the emission spectrum at
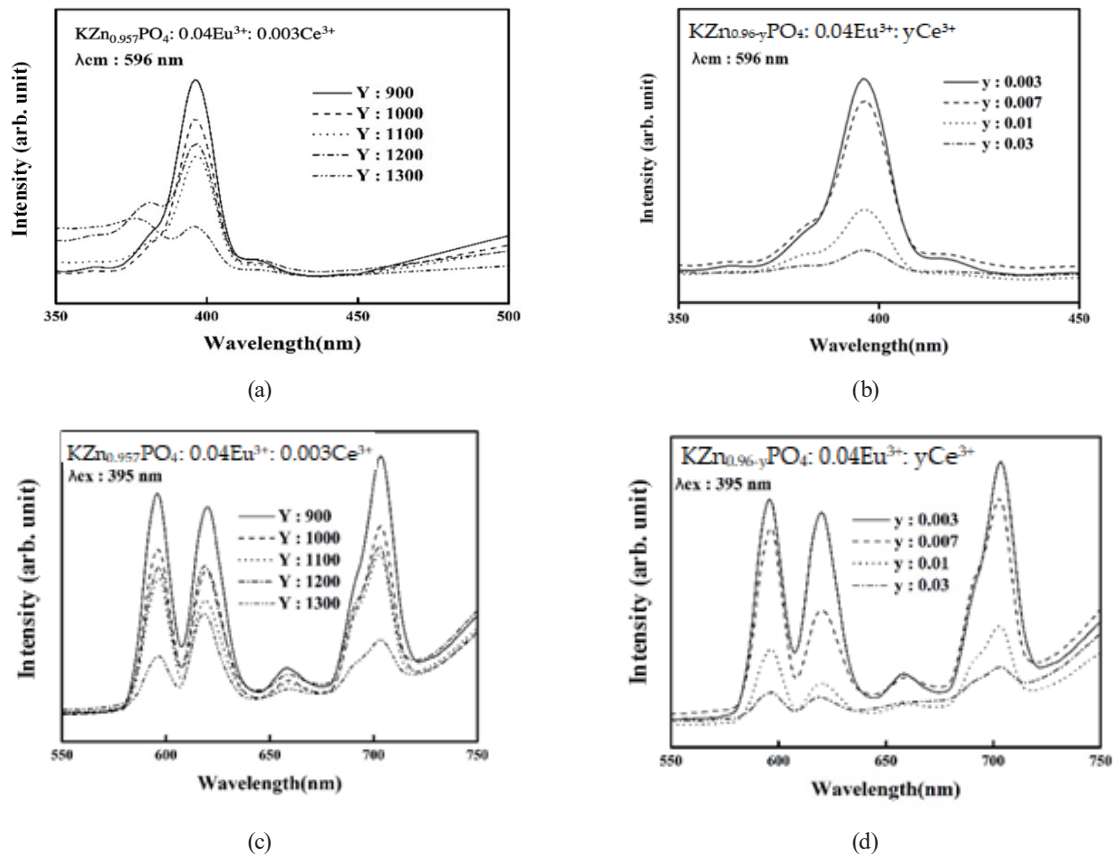

Fig. 4. (a) PL excitation spectra of $KZn_{0.957}PO_4:0.04Eu^{3+}:0.003Ce^{3+}$ phosphor sintered at 900, 1000, 1100, 1200, and 1300 °C (λ_{em} = 596 nm). (b) PL excitation spectra of $KZn_{0.96-y}PO_4:0.04Eu^{3+}:yCe^{3+}$ phosphors with different Ce^{3+} concentrations sintered at 900 °C (λ_{em} = 596 nm). (c) PL emission spectra of $KZn_{0.957}PO_4:0.04Eu^{3+}:0.003Ce^{3+}$ phosphors sintered at 900, 1000, 1100, 1200, and 1300 °C (λ_{ex} = 395 nm). (d) PL emission spectra of $KZn_{0.96-y}PO_4:0.04Eu^{3+}:yCe^{3+}$ (y = 0.003, 0.007, 0.01, and 0.03) phosphors sintered at 900 °C (λ_{ex} = 395 nm).

room temperature. In Ref. 15, for $KZnPO_4:Eu^{3+}$, the peak related to the intraconfigurational 4f–4f transitions of Eu^{3+} was reported to be clear and distinct. However, in this study, the peaks from the intraconfigurational 4f–4f transitions of Eu^{3+} seem to overlap each other to form a broadband owing to the codoping effect of Ce^{3+}. This result was different from the report[25] in which it was suggested that there is no possibility for energy transfer from Ce^{3+} to Eu^{3+} or vice versa because Ce^{3+}/Eu^{3+} is not a good sensitizer/activator pair. Additionally, along with increasing sintering temperature, the peak intensity at around 394 nm decreased owing to bad particle morphology.[26] Figure 4(b) shows the PL excitation spectra of $KZn_{0.96-y}PO_4:0.04Eu^{3+}:yCe^{3+}$ phosphors with $y = 0.003, 0.007, 0.01$, and 0.03 sintered at 900 °C. As to the prominent excitation peak at 394 nm, when the codoping concentration increases, the peak intensity reduction may result from the lattice distortion indicated by the XRD diffraction peak shifts. Figure 4(c) shows the PL emission spectra of $KZn_{0.957}PO_4:0.04Eu^{3+}:0.003Ce^{3+}$ synthesized at different temperatures. Additionally, Fig. 4(d) shows the PL emission spectra of $KZn_{0.96-y}PO_4:0.04Eu^{3+}:yCe^{3+}$ ($y = 0.003, 0.007, 0.01$, and 0.03) phosphors sintered at 900 °C (λ_{ex} = 395 nm). The spectra comprise several sharp lines ranging from 575 to 710 nm, and they correspond to the transitions from the excited state $^5D_0$ to ^7F_J ($J = 0, 1, 2, 3$, and 4) of Eu^{3+}. The emission peaks are located at 596 nm ($^5D_0 \rightarrow {}^7F_1$ magnetic transition), 615 nm ($^5D_0 \rightarrow {}^7F_2$ electronic transition), 655 nm ($^5D_0 \rightarrow {}^7F_3$ magnetic transition), and 700 nm ($^5D_0 \rightarrow {}^7F_4$ electronic transition).[27–29] In our previous study,[15] we observed that $KZn_{1-x}PO_4:xEu^{3+}$ phosphors emit orange-red light (596 nm) because of the dominant $^5D_0 \rightarrow {}^7F_1$ transitions. However, in this study, the red-light components from 615 nm ($^5D_0 \rightarrow {}^7F_2$) and 700 nm ($^5D_0 \rightarrow {}^7F_4$) are dominant. As we know, the asymmetry ratio (A_{21}), which is defined as $A_{21} = I_2$ ($^5D_0 \rightarrow {}^7F_2)/I_1$ ($^5D_0 \rightarrow {}^7F_1$), is used to illustrate the environmental change around Eu^{3+} ions in the $KZnPO_4$ system.[14,30] If the intensity of the emission peaks located at 596 nm ($^5D_0 \rightarrow {}^7F_1$ magnetic transition) is higher than that of the peak at 615 nm ($^5D_0 \rightarrow {}^7F_2$ electronic transition), a higher symmetry of the crystal field around Eu^{3+} is expected. $KZnPO_4$ doped only with Eu^{3+} mainly emits 593 nm orange light ($^5D_0 \rightarrow {}^7F_1$), indicating that Eu^{3+} occupies the crystallographic sites with a symmetric inversion center. However, in this study, the red light of 618 nm ($^5D_0 \rightarrow {}^7F_2$) and 700 nm ($^5D_0 \rightarrow {}^7F_4$) is dominant because of the lattice distortion effect resulting in different crystal fields in the Eu/Ce codoped $KZnPO_4$ system.[31,32] Our result is opposite to that in Ref. 11, in which Ce^{3+} was reported to enhance the symmetry around the Eu^{3+} ions in the Eu/Ce codoped Li_2BaZrO_4 system. The same doping species in different host lattices causes very different effects.

Figure 5 shows the Commission Internationale de I'Edairage CIE chromaticity coordinates with different color tones for $KZn_{0.957}PO_4:0.04Eu^{3+}:0.003Ce^{3+}$ phosphors excited at 395 nm. The chromaticity (x, y) coordinates of the $KZn_{0.957}PO_4:0.04Eu^{3+}:0.003Ce^{3+}$ phosphors appear in the red region (0.74, 0.27). Table 1 lists the chromaticity (x, y) coordinates of the $KZn_{1-x-y}PO_4:0.04Eu^{3+}:yCe^{3+}$ phosphors with different doping levels and synthesis conditions. Only the synthesis conditions affect the chromaticity (x, y) coordinates of the $KZn_{1-x-y}PO_4:0.04Eu^{3+}:yCe^{3+}$ phosphors from the region (0.73, 0.27) to (0.69, 0.31) owing to melting.

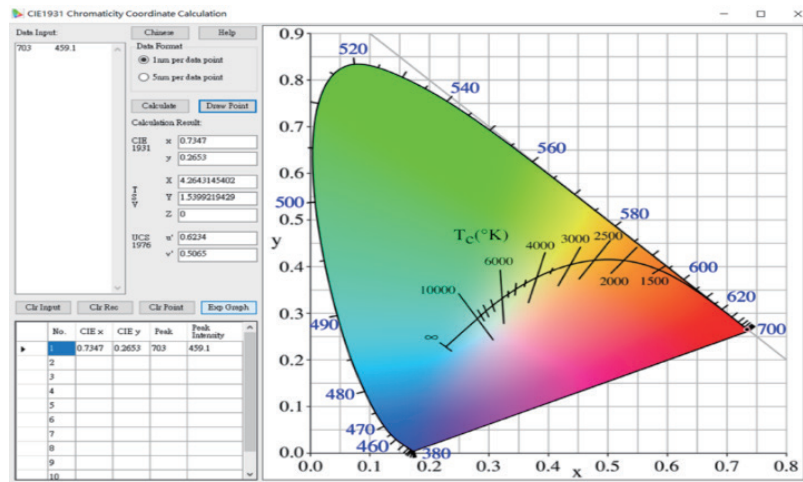Fig. 5.   (Color online) CIE-1931 chromaticity diagram of $KZn_{0.957}PO_4{:}0.04Eu^{3+}{:}0.003Ce^{3+}$ phosphors sintered at 900 °C (λ_{ex} = 395 nm).

Table 1
Chromaticity coordinates of $KZn_{1-x-y}PO_4{:}0.04Eu^{3+}{:}yCe^{3+}$ phosphors with different doping concentrations and synthesis conditions.

No.	$KZn^{0.957}$ PO_4: $0.04Eu^{3+}$: $0.003Ce^{3+}$ sintered at 900 °C	$KZn^{0.957}$ PO_4: $0.04Eu^{3+}$: $0.003Ce^{3+}$ sintered at 1000 °C	$KZn^{0.957}$ PO_4: $0.04Eu^{3+}$: $0.003Ce^{3+}$ sintered at 1100 °C	$KZn^{0.957}$ PO_4: $0.04Eu^{3+}$: $0.003Ce^{3+}$ sintered at 1200 °C	$KZn^{0.957}$ PO_4: $0.04Eu^{3+}$: $0.003Ce^{3+}$ sintered at 1300 °C	$KZn^{0.96-y}$ PO_4: $0.04Eu^{3+}$: yCe^{3+} $y = 0.007$ sintered at 900 °C	$KZn^{0.96-y}$ PO_4: $0.04Eu^{3+}$: yCe^{3+} $y = 0.01$ sintered at 900 °C	$KZn^{0.96-y}$ PO_4: $0.04Eu^{3+}$: yCe^{3+} $y = 0.03$ sintered at 900 °C
CIE, x	0.73	0.73	0.73	0.73	0.69	0.73	0.73	0.73
CIE, y	0.27	0.27	0.27	0.27	0.31	0.27	0.27	0.27

5.   Conclusions

A series of $KZn_{0.96-y}PO_4{:}0.04Eu^{3+}{:}yCe^{3+}$ (y = 0.003, 0.007, 0.01, and 0.03) phosphors were successfully synthesized by the solid-state reaction and their luminescent properties were investigated. There was no change in crystal structure type upon codoping, and the $KZnPO_4$ single phase was confirmed. Under the excitation of 394 nm, the dominance of the electronic dipole transition related to red light emission at 618 nm ($^5D_0 \rightarrow {}^7F_2$) and 700 nm ($^5D_0 \rightarrow {}^7F_4$) in $KZnPO_4{:}Ce^{3+},Eu^{3+}$ phosphors confirmed the asymmetry around the Eu^{3+} ion. The primary reason for the different emission properties is that the codoping of these rare-earth ions of different ionic sizes resulted in microstructural reconstruction. Therefore, different host materials with various crystal fields and different heating mechanisms that may result in additional energy transfer methods of the phosphors could affect the fluorescent properties of the phosphors. Additionally, codoping may be a convenient process of adjusting the luminescence characteristics of the phosphors.

Acknowledgments

Author Contribution

Conceptualization: Guan Ping Qi; Materials analysis and data collection: Huang Sheng Lai; Data organization and execution of experiment: Shoou-Jinn Chang; Validation and formal analysis: Ru-Yuan Yang; Structure analysis, theory confirmation, formulate confirmation, and final structure verification: Professor Ru-Yuan Yang.

References

1 M. Xia, Z. Ju, H. Yang, Z. Wang, X. Gao, and F. Pan: J. Alloys Compd. **73** (2018) 439. https://www.sciencedirect.com/science/article/pii/S0925838817344389?via%3Dihub

2 Z. Xia, Y. Zhang, M. S. Molokeev, and V. V. Atuchin: J. Phys. Chem. C **117** (2013) 20847. https://doi.org/10.1021/jp4062225

3 V. V. Atuchin, N. F. Beisel, E. N. Galashov, E. M. Mandrik, M. S. Molokeev, and A. P. Yelisseyev: ACS Appl. Mater. Interfaces **7** (2015) 26235. https://doi.org/10.1021/acsami.5b08411

4 J. L. Leaño Jr, S.-Y. Lin, A. Lazarowska, S. Mahlik, M. Grinberg, and C. Liang: Chem. Mater. **28** (2016) 6822. https://doi.org/10.1021/acs.chemmater.6b03442

5 H. Luo, J. Liu, X. Zheng, L. Han, K. Ren, and X. Yu: J. Mater. Chem. A **22** (2012) 15887. https://pubs.rsc.org/en/content/articlelanding/2012/jm/c2jm32293e

6 S. Ramteke, A. Yerpude, N. Kokode, and S. Dhoble: Bull. Mater. Sci. **44** (2021) 174. https://doi.org/10.1007/s12034-021-02476-5

7 J. N. Keil, H. Jenneboer and T. Jüstel: J. Lumin. **238** (2021) 118307. https://www.sciencedirect.com/science/article/pii/S0022231321004233

8 V. Singh, C. B. A. Devi, A. Rao, and J. Rao: Optik **208** (2020) 163632. https://www.sciencedirect.com/science/article/pii/S003040261931530X

9 M. Nazarov, J. Sohn, and C. Yoon: Opt. Mater. **30** (2008) 1387. https://www.sciencedirect.com/science/article/pii/S0925346707002467

10 C. Ye: J. Lumin. **213** (2019) 75. https://www.sciencedirect.com/science/article/pii/S0022231319301395

11 I. Ahemen and F. Dejene: J. Alloys Compd. **735** (2018) 2436. https://www.sciencedirect.com/science/article/pii/S0925838817341944

12 F. Meng, H. Zhang, C. Chen, S. I. Kim, H. J. Seo, and X. Zhang: J. Alloys Compd. **671** (2016) 150. https://www.sciencedirect.com/science/article/pii/S0925838816303553

13 A. Zou, S. Sun, J. Yu, N. Zou, Z. Hu, and Y. Zhang: J. Mater. Sci.: Mater. Electron. **30** (2019) 9155. https://doi.org/10.1007/s10854-019-01244-w

14 Y. Chen, H. Weng, J. Chang, and Y. Yang: Ceram. Int. **38** (2012) 125. https://www.sciencedirect.com/science/article/pii/S027288421100589X

15 M. Weng, C. Liauh, Y. Peng, J. H. Chen, and R. Yang: Materials (2022).

16 G. Wallez, F. Lucas, J. P. Souron, and M. Quarton: Mater. Res. Bull. **34** (1999) 1251. https://www.sciencedirect.com/science/article/pii/S0025540899001245

17 V. Atuchin, T. Gavrilova, C. Grivel, and V. Kesler: J. Phys. D: Appl. Phys. **42** (2008) 035305. https://doi.org/10.1088/0022-3727/42/3/035305

18 C. S. Lim, A. Aleksandrovsky, M. Molokeev, A. Oreshonkov, and V. Atuchin: Chem. Phys. **17** (2015) 19278. https://pubs.rsc.org/en/content/articlehtml/2015/cp/c5cp03054d

19 V. Atuchin, A. Subanakov, A. Aleksandrovsky, B. Bazarov, J. Bazarova, and S. Dorzhieva: Adv. Powder Technol. **28** (2017) 1309. https://www.sciencedirect.com/science/article/pii/S0921883117300973

20   G. Jyothi, L. S. Kumari, and K. Gopchandran: Ceram. Int. **43** (2017) 12044. https://www.sciencedirect.com/science/article/pii/S0272884217312737
21   S. Zhang, Y. Huang, and H. J. Seo: J. Electrochem. Soc. **157** (2010) J261. https://doi.org/10.1149/1.3429887/meta
22   P. Shi, Z. Xia, S. Molokeev, and V. Atuchin: Dalton Trans. **43** (2014) 9669. https://pubs.rsc.org/en/content/articlehtml/2014/dt/c4dt00339j
23   H. Ji, Z. Huang, Z. Xia, S. Molokeev, X. Jiang, and Z. Lin: Dalton Trans. **44** (2015) 7679. https://pubs.rsc.org/en/content/articlelanding/2015/dt/c4dt03887h
24   L. Van: J. Electrochem. Soc. **114** (1967) 1048. https://doi.org/10.1149/1.2424184/meta
25   S. Singh, G. Lakshminarayana, M. Sharma, T. D. Dao, K. Chen, and Y. Wada: J. Spectrosc. **2015** (2015). https://www.hindawi.com/journals/jspec/2015/493607/
26   V. Bandi, Y. Nien, T. Lu, and I. Chen: J. Am. Ceram. Soc. **92** (2009) 2953. https://doi.org/10.1111/j.1551-2916.2009.03308.x
27   V. Atuchin, A. Aleksandrovsky, O. Chimitova, T. Gavrilova, A. Krylov, and M. Molokeev: J. Phys. Chem. C **118** (2014) 15404. https://doi.org/10.1021/jp5040739
28   V. Atuchin, A. Subanakov, A. Aleksandrovsky, B. Bazarov, J. Bazarova, and T. Gavrilova: Mater. Des. **140** (2018) 488. https://www.sciencedirect.com/science/article/pii/S0264127517311097
29   Y. Denisenko, V. Atuchin, S. Molokeev, S. Aleksandrovsky, S. Krylov, and S. Oreshonkov: Inorg. Chem. **57** (2018) 13279. https://doi.org/10.1021/acs.inorgchem.8b01837
30   R. Yang, Y. Peng, H. Lai, Y. Su, and S. Chang: Ceram. Int. **43** (2017) S682. https://www.sciencedirect.com/science/article/pii/S0272884217310842
31   G. Lakshminarayana and S. Buddhudu: Mater. Chem. Phys. **102** (2007) 181. https://www.sciencedirect.com/science/article/pii/S0254058406003105
32   M. Dousti, A. Molla, A. Rodrigues, and A. de Camargo: Opt. Mater. **69** (2017) 372. https://www.sciencedirect.com/science/article/pii/S0925346717302756

About the Authors

Guan-Ping Qi received his M.S. degree in material fields from the National Pingtung University of Science and Technology in 2012. He is currently a Ph.D. candidate at the Institute of Microelectronics, National Cheng Kung University in Taiwan. From 2019 to 2024, he was the chairman of Metalcobalt Company in Taiwan. His research interests are in developing and investigating dry pumps and graphite materials for semiconductors. (a72190639@gmail.com, metalcobalt27@gmail.com)

Huang Sheng Lai received his B.S. degree from the National Sun Yat-sen University, Taiwan, in 2022 and M.S. degree from the National Pingtung University of Science and Technology, Taiwan, in 2024. (a9507012@gmail.com)

Shoou-Jinn Chang received his B.S. degree from National Cheng Kung University, Taiwan, in 1983, M.S. degree from Stony Brook University, USA, in 1985, and Ph.D. from the University of California, USA, in 1989. From 1992 to 1998, he was a professor at the Institute of Microelectronics, National Cheng Kung University, Taiwan. Since 2016, he has been a chair professor at the same university. (changsj@mail.ncku.edu.tw)

Ru-Yuan Yang received his B.S. degree from National Taiwan Normal University, Taiwan, and M.S. and Ph.D degrees from National Sun Yat-sen University and National Cheng Kung University, respectively. (ryyang@mail.npust.edu.tw)